Received: 10 October 2018 | Revised: 19 December 2018 | Accepted: 20 December 2018

DOI: 10.1111/bre.12335

ORIGINAL ARTICLE

WILEY Basin Research IAS EAGE

Discrete element modelling of extensional, growth, fault-propagation folds

Stuart Hardy[1,2]

[1]ICREA (Institució Catalana de Recerca i Estudis Avançats), Barcelona, Spain

[2]Facultat de Geologia, Universitat de Barcelona, Barcelona, Spain

Correspondence
Stuart Hardy, Facultat de Geologia, Universitat de Barcelona, Barcelona, Spain.
Email: stuart.hardy@icrea.cat

Abstract

Extensional fault-propagation folds are now recognised as being an important part of basin structure and development. They have a very distinctive expression, often presenting an upward-widening monocline, which is subsequently breached by an underlying, propagating fault. Growth strata, if present, are thought to provide a crucial insight into the manner in which such structures grow in space and time. However, interpreting their stratigraphic signal is neither straightforward nor unique. Both analogue and numerical models can provide some insight into fold growth. In particular, the trishear kinematic model has been widely adopted to explain many aspects of the evolution and geometry of such fault-propagation folds. However, in some cases the materials/rheologies used to represent the cover do not reproduce the key geometric/stratigraphic features of such folds seen in nature. This appears to arise from such studies not addressing adequately the very heterogenous mechanical stratigraphy seen in many sedimentary covers. In particular, flexural slip between beds/layers is often not explicitly modelled but, paradoxically, it appears to be an important deformation mechanism operative in such settings. Here, I present a 2D discrete element model of extensional fault-propagation folding which explicitly includes flexural slip between predefined sedimentary units or layers in the cover. The model also includes growth strata and shows how they may reflect the various evolutionary stages of fold and fault growth. When flexural slip is included in the modelling scheme, the resultant breached monoclines and their growth strata are strikingly similar to some of those seen in nature. Results are also compared with those obtained using simple, homogeneous, frictional-cohesive and elastic cover materials. Both un-lithified and lithified growth strata are considered and clearly show that, rather than just being passive recorders of structural evolution, growth strata can *themselves* have an important effect on fault-related fold growth. Implications for the evolution of and strain within, the resultant growth structures are discussed. A final focus of this study is the relationship that trishear might have with the upward-widening zone of flexural slip activation away from a fault tip singularity.

1 | INTRODUCTION

Geological structures in sedimentary basins are rarely simple and much of their complexity arises from the stratigraphic and thus mechanical, heterogeneity of the crustal section being deformed. Such heterogeneity is now acknowledged as being of great importance in the evolution of faults and folds. Of particular interest here, folding ahead of upward propagating faults is now recognised as being an important process in extensional basins. Such folds have a rather

varied nomenclature in the literature: precursor folds, monoclines, forced folds, extensional fault-propagation folds, etc. However, overall, they have very distinctive geometries observed both in the field and on seismic (Figure 1a–c). Early in their evolution they are typically single-limbed folds (monoclines), which are associated with the tips of normal faults (e.g. Keller & Lynch, 2000; Sharp, Gawthorpe, Underhill, & Gupta, 2000; Willsey, Umhoefer, & Hilley, 2002; Grant & Kattenhorn, 2004; Jackson, Gawthorpe, & Sharp, 2006; White & Crider, 2006). Once breached by the propagating fault, they often show distinctive hanging-wall synclines and minor footwall anticlines. Growth strata, where present, often exhibit a distinctive thinning towards the fault-related fold early in its evolution, whereas later growth strata are either parallel or may *thicken* towards the fault (Figure 1c). The formation and geometry of such folds has been extensively studied from outcrop (Ferrill & Morris, 2008; Ferrill, Morris, & Smart, 2007; Jackson et al., 2006; Sharp et al., 2000; White & Crider, 2006), physical analogue models (Withjack & Calloway, 2000; Withjack, Olson, & Peterson, 1990), numerical models (Hardy & McClay, 1999; Jin & Groshong, 2006; Patton, 2004; Willsey et al., 2002) and from seismic reflection data (Ford, Carlier, Veslud, & Bourgeois, 2007; Kane, Jackson, & Larsen, 2010; Keller & Lynch, 2000; Lewis, Jackson, & Gawthorpe, 2013; Maurin & Niviere, 2000; Pascoe, Hooper, Storhaug, & Harper, 1999). There are undoubtedly many different factors that control the geometry of fault-propagation folds. However, the mechanical stratigraphy of the folded cover sequence has been identified as a primary control with strong mechanical contrasts between layers allowing shear/slip along bedding planes to accommodate folding (Ferrill & Morris, 2008; Ferrill, Morris, & McGinnis, 2012; Ferrill et al., 2007; Jackson et al., 2006; Lăpădat et al., 2016; Smart & Ferrill, 2018). Similarly, large mechanical contrasts between rigid basement and an overlying, weaker cover may lead to decoupling and folding of the cover sequence (Ford et al., 2007; Kane et al., 2010; Lewis et al., 2013; Pascoe et al., 1999; Sharp et al., 2000; Tvedt, Rotevatn, Jackson, Fossen, & Gawthorpe, 2013; Withjack & Calloway, 2000).

Previous mechanical numerical modelling studies of extensional fault-related folding have either not addressed the importance of flexural-slip (Finch, Hardy, & Gawthorpe, 2004; Patton, 2004) or, when considering mechanical heterogeneity have been at a small scale (10–100s of metres; Schopfer, Childs, & Walsh, 2007; Smart, Ferrill, & Morris, 2009; Smart et al., 2010; Smart & Ferrill, 2018), or have not permitted breaching of the monocline by fault propagation (Johnson & Johnson, 2002a, 2002b; Smart et al., 2010). Furthermore, no previous studies have considered the development of an extensional fault-propagation fold and associated growth strata at a kilometric scale. In addition, as regards kinematic models, over the past 20 years the trishear model has been widely adopted to explain many aspects of the geometry of such fault-propagation folds (Allmendinger, 1998; Erslev, 1991; Hardy & McClay, 1999; Jin & Groshong, 2006; Khalil & McClay, 2002; Zhao, Guo, & Yu, 2017). However, whilst trishear clearly produces early monoclines and later breached folds with a *geometric* similarity to those seen in nature, relating trishear to field observations of deformation is neither simple nor straightforward. As such, the geological significance of the trishear model (like many kinematic models) is not fully understood (e.g. Allmendinger, 1998; Cardozo, Jackson, & Whipp, 2011). To complement these studies, here I use a discrete element model to investigate the evolution of extensional fault-propagation folds. The model builds on previous work by explicitly simulating flexural slip between multiple layers in the cover and these models replicate well the geometries typically seen in nature. Results are also compared with those obtained using simple, homogeneous, frictional-cohesive and elastic bonded cover materials. The model also includes growth strata and shows how they may reflect the various stages of fold and fault growth. Differences between models including unlithified and lithified growth strata clearly show the effect that growth strata *themselves* can have on fault-related fold geometries; they are perhaps much more than just passive recorders of tectonic activity. The implications of the model results for the interpretation of folds and growth strata sequences seen in nature and in seismic and the application of kinematic models to such structures are discussed.

Highlights

- Novel discrete element approach to modelling extensional fault-propagation folds.
- Inclusion of flexural slip reproduces typical natural examples.
- Complex growth sequences reflect fold and fault growth.
- Growth sedimentation not only records but also influences fault-related fold growth.

2 | METHODOLOGY

Here I use a discrete element numerical model to simulate the growth of extensional fault-propagation folds and their associated growth strata. The discrete element code used here to undertake these simulations is ¨cdem2D¨ which has been used previously to undertake a wide variety of structural geology modelling in both 2D and 3D (as cdem3D). The basic numerical methodology

and its application to a variety of problems (fault-propagation folding, orogenic wedge growth, caldera collapse, dike intrusion on Mars, viscous flow, Gilbert deltas, etc.) have been published previously (e.g. Botter, Cardozo, Hardy, Lecomte, & Escalona, 2014; Botter et al., 2016; Hardy, 2008; Hardy, McClay, & Muñoz, 2009; Hardy, 2016; Hardy, 2018a, 2018b). Of particular interest here, the details of this code applied to elastic and cohesive-frictional materials can be found elsewhere (e.g. Hardy et al., 2009; Hardy, 2011, 2015), however an overview is given below. Here, I will illustrate the use of this modelling scheme to include flexural-slip and to simulate growth sedimentation associated with active extensional fault-propagation folding.

The discrete element technique, in common with other numerical techniques, has both advantages and disadvantages when considering its application to any geological problem. Modelling of deformation to high strain is an ideal candidate for its use as it is well-suited to studying problems in which discontinuities (shear-zones, faults, fractures etc) are important. It also allows deformation involving unlimited relative motions of individual elements and complex, abrupt and changing boundary conditions (Cundall & Strack, 1979; Egholm, Sandiford, Clausen, & Nielsen, 2007; Finch et al., 2004; Hardy, 2008, 2011; Thompson, Bennett, & Petford, 2010). However, one disadvantage of the technique lies in the necessary, but time-consuming, calibration of micro-particle parameters to physical properties (cf. Egholm et al., 2007; Botter et al., 2014). The interactions of many tens of thousands of particles, both locally and globally, also lead to situations wherein our ability to explain precisely *why* a particular fault or fracture grew at the expense of a neighbouring one is limited. Such issues also exist in analogue modelling where repeated experiments under the same boundary conditions are reasonably reproducible but not in the finer details of the fault and fracture systems (e.g. van Gent et al., 2010). Computational limitations on element size and/or model resolution, whilst important previously, are now no longer a particular concern due to recent rapid advances in computational power and the parallelisation of many discrete element codes.

The discrete-element model described here is a variant/development of the lattice solid model (LSM; Mora & Place, 1993, 1994; Place, Lombard, Mora, & Abe, 2002). A rock, or sedimentary, mass is treated as an assemblage of circular elements, which interact as if connected by breakable elastic springs (bonds) and that undergo motion relative to one another. The behaviour of the elements assumes that the particles interact through a 'repulsive–attractive' force (Mora & Place, 1993) in which the resultant (normal) force, F_n, is given by.

$$\begin{aligned} F_n &= K_n(r-R) \quad r < r_0 \text{ intact bond} \\ F_n &= K_n(r-R) \quad r < R \text{ broken bond} \\ F_n &= 0 \qquad\quad r \geq R \text{ broken bond} \end{aligned} \tag{1}$$

Here, K_n is the elastic constant (normal spring stiffness) of the bond, R is the equilibrium distance between the particles (sum of particle radii), r_0 is a breaking threshold and r is the current distance between the particle pair. Particles within the model assemblage are bonded until the distance (r) between them exceeds the defined breaking threshold at which time the bond breaks; in un-bonded assemblages all bonds are initially broken. The force acting on a bond at this threshold represents the force necessary for a bond to fail or yield, or, alternatively, can be cast as the stress acting on a particle's bond at failure. After this breaking threshold, the particle pair experiences no further attractive force and the bond is irreversibly broken. However, if the two particles return to a compressive contact, a repulsive force still acts between them.

For a *frictional-cohesive* material, in addition to treating the normal force (F_n) between particles, I also calculate the tangential (shear) force, F_S, as a result of displacement (X_s) perpendicular to the vector connecting the particles' centroids. This frictional force acts in a direction opposite to that of the relative tangential velocity and is modelled as a threshold-limited elastic spring with a cohesive force term (C_0) in parallel with that used to calculate the normal forces (cf. Cundall & Strack, 1979; Mora & Place, 1994). The magnitude of this force is limited to be less than or equal to the shear force allowed by Coulomb friction:

$$\begin{aligned} F_s &= K_s X_s + C_0 \\ F_{s\max} &= \mu F_n \\ F_s &= F_{s\max} \text{ if } \left(F_s > F_{s\max}\right) \end{aligned} \tag{2}$$

where K_s is the elastic constant (shear spring stiffness) of the contact, F_{Smax} is the maximum (limiting) shear (frictional)

FIGURE 1 (a) Outcrop of a breached fault-propagation fold from the Suez rift, Egypt (after Withjack et al., 1990; pC— Precambrian, PKn—Carboniferous, Upper Cretaceous, Kum—Upper Cretaceous, Kuc—Upper Cretaceous, Paleocene, Te—Eocene, Tmp Miocene, Pliocene, Holocene); (b) detail of Miocene growth-strata from theWadi Baba area, Suez rift, illustrating progressive decrease in amount of rotation. Normal fault is located on the right of the photograph and the cliff face is approximately 150 m high; (c) Schematic diagram of the evolution from a monocline above a buried, active normal fault to the eventual breaching of the monocline. This process results in an early synrift sequence that onlaps and thins towards the monocline overlain by a later synrift sequence that thickens towards the emergent fault. Based on field examples from the Sinai margin of the Gulf of Suez; approximate horizontal scaled indicated. Redrawn from Gawthorpe *et al*. (1997). (d) Initial configuration of the discrete element model used in the simulations presented here—an identical crustal section 6.25 km by 2.77 km is underlain by a basement normal fault dipping at 70 degrees. (e) Uniaxial unconfined compressive tests of three rheologies used in the models presented here

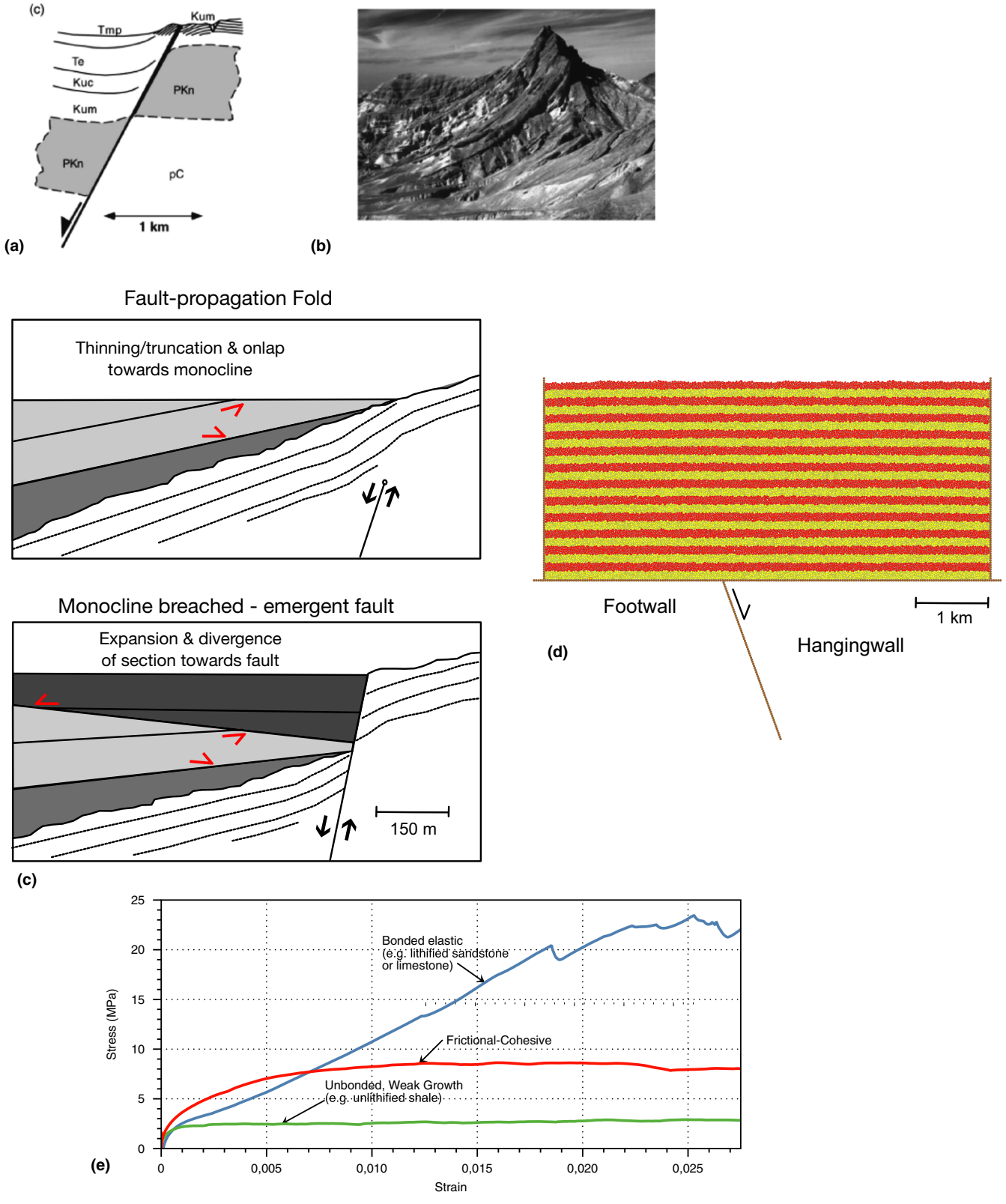

force, F_n is the normal force at a contact and μ is the inter-particle coefficient of friction. If a contact is 'lost' between two touching elements (i.e. they separate), then all the forces between the elements are set to zero. The total elastic force, $F_{i,a}$ exerted on a particle is thus obtained by summing the normal and tangential forces on each contact/bond that links a specific particle to its a neighbours, calculated by

$$F_{i,\alpha} = \sum_{j=1,\alpha} f_{i,j} \tag{3}$$

where $f_{i,j}$ is the elastic force (normal and shear) experienced by particle i from its neighbouring particle j. However, we include a viscous damping term (proportional to particle velocity) that acts to dampen reflected waves from the rigid edges/boundaries of our model, preventing a build-up of kinetic energy within the closed system, a standard technique to ensure numerical stability (cf. Mora & Place, 1994; Place et al., 2002).

Finally, gravitational forces, F_g, acting on each element are calculated in the z direction, increasing the vertical stress with depth. Therefore, the total force (F) on any particle is given by

$$F = F_{i,\alpha} - v\dot{x} + F_g \quad (4)$$

where v represents the dynamic viscosity and x is the velocity of the particle. At each discrete time step, the particles are advanced to their new positions within the model by integrating their equations of motion using Newtonian physics and a velocity-Verlet-based scheme (Allen & Tildesley, 1987). In discrete element models such as that used here parameters such as strength, coefficient of friction etc, of an assemblage are emergent properties and do not relate directly to micro-properties. They are typically assessed through the use of angle of repose and/or unconfined/confined biaxial numerical tests (cf. Oger, Savage, Corriveau, & Sayed, 1998; Finch et al., 2004; Holohan, Schopfer, & Walsh, 2011; Botter et al., 2014).

The key additional feature presented here is that, unlike simple homogeneously bonded discrete element assemblages, we can choose to have element bonding only activated *within* (a set of predefined) layers and not *between* these layers. I incorporate this heterogeneous layering into the models in order to facilitate flexural slip deformation along layer interfaces and thus better approximate the typically anisotropic mechanical stratigraphy of sedimentary cover rocks, be this a layered sandstone-shale sequence or salt layers etc. These inter-layer contacts have no cohesive bonds or friction, in order to make these interfaces as weak as possible. The interfaces cannot be frictionless in the true sense, due to the 'roughness' of circular elements and thus there is always some residual, intrinsic friction at the interface; it remains much weaker than a frictional or bonded interface nonetheless. All other numerical techniques and approaches used on the elements are identical to those discussed in previous papers to which the interested reader is referred (e.g. Hardy et al., 2009; Hardy, 2011, 2015). A second feature to be presented here is the use of the discrete element technique not *only* to model deformation of a pre-existing sedimentary sequence but also to model the deposition (and subsequent deformation) of a growth sedimentary sequence deposited during active tectonics. After growth sediments are added to an evolving model, these elements must be allowed to equilibrate/adjust to a final, initial deposited state. This is done by pausing any external boundary movement after discrete element addition for a predefined (very small) number of time-steps until the added elements are in a quasi-static location and effectively stable. The model then continues as before but with a new sediment load added to the system; compaction per se is not considered, but the increased load, as a result of sedimentation, changes forces and element packing at depth. The specific heuristic used here is to add discrete elements of variable size (average radius c. 9.5 m), filling up any available submarine accommodation space. These elements are chosen randomly and then added sequentially with each additional element attempting to minimise the remaining accommodation space until it is filled. They are carefully placed to ensure that they maximise the filling of available accommodation space while just touching pre-existing deposited elements. These growth elements can either be un-bonded to represent weak, unconsolidated (un-lithified) sediments or can be bonded/cohesional to represent rapidly lithified (via compaction or cementation and thus much stronger) growth strata. I do not consider the transport of these elements above sea level or their erosion in this study. The spatial resolution chosen here is arbitrary but it is appropriate to introduce the approach and to achieve realistic runtimes, with today's rapid advances in computing power model resolution is becoming less and less of an issue.

2.1 | Model parameters, set-up and boundary conditions

Below I present the results of three simple two-dimensional numerical models (experiments) of growth, extensional fault-propagation folding. I firstly examine the growth of a fault-propagation fold in a cover section which is simply frictional-cohesive (Figure 2), then examine the growth of a fault-propagation fold in a cover which is homogenous, bonded elastic (Figure 3) and finally a cover that is bonded elastic within layers but unbonded between them to simulate flexural slip (Figure 4). Growth strata in these initial models are considered to be un-lithified and thus very weak. Therefore these discrete elements are considered to be purely elastic and are neither bonded nor frictional-cohesive. In each case I examine the growth of an extensional fault-related fold in an identical crustal section with dimensions of 6.25 km by 2.77 km, above a basement normal fault dipping at 70 degrees (Figure 1d), values chosen to encapsulate typical field and seismic examples. The model represents the pregrowth section (the sedimentary cover above the basement) of the upper crust using approximately 46,000 elements. After incrementally adding growth strata, the final models in each experiment are

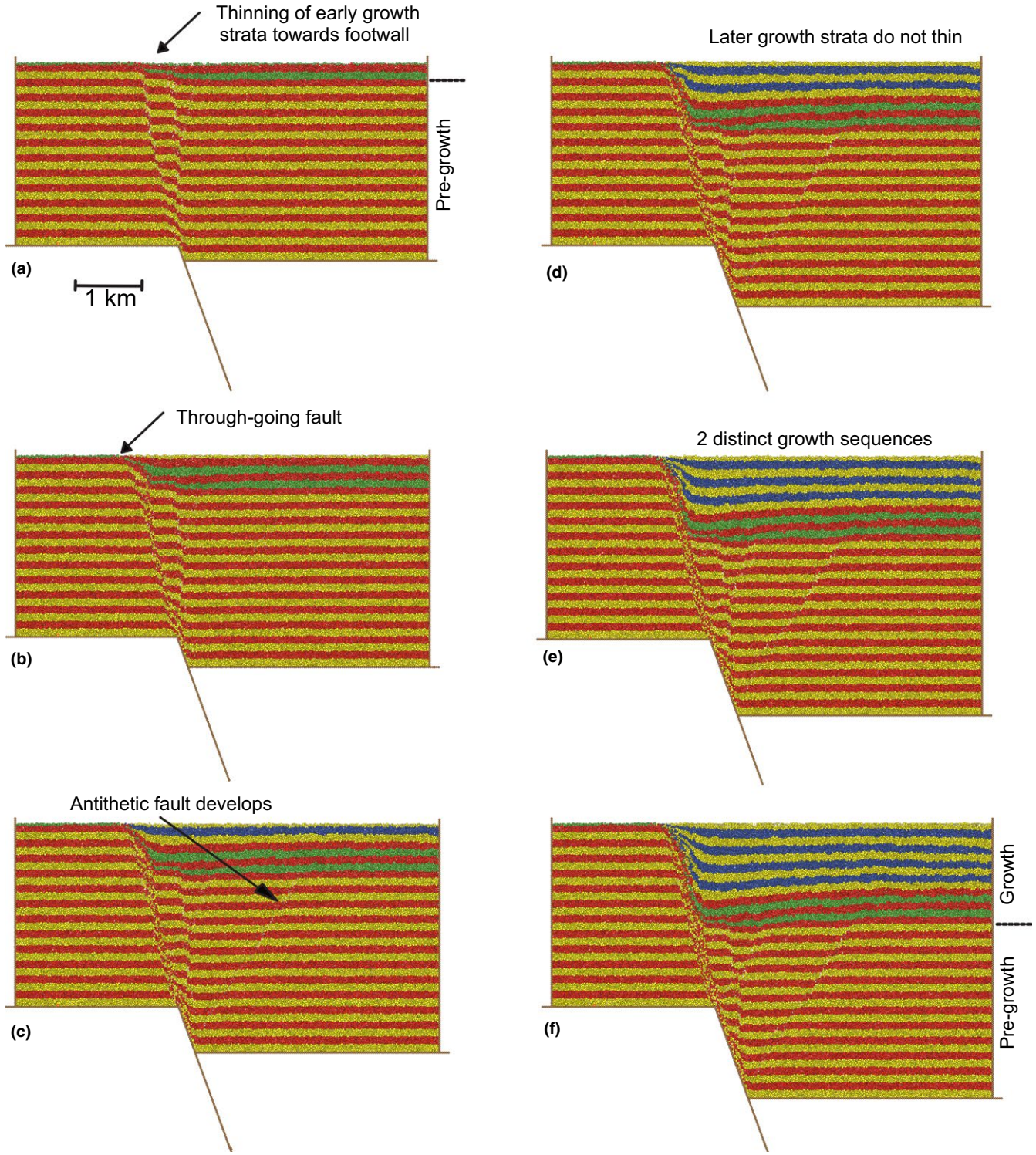

FIGURE 2 Experiment 1: a simple frictional-cohesive fault-propagation simulation. Model results shown at (a) 250, (b) 500, (c) 750, (d) 1,000, (e) 1,250 and (f) 1,500 m displacement on basement fault. Distance scale shown, no vertical exaggeration. Pregrowth strata are coloured yellow and red. Two growth strata sequences are highlighted; an early package (coloured green and red) and a later one (coloured yellow and blue)

composed of approximately 100,000 elements. Element radii range from 6.25 to 15.625 m (average radius 9.5 m) and their density is 2,500 kg/m^3. Here, I choose to define both pregrowth and growth layers as being approximately 55 m thick, this value is arbitrary but shows the manner in which flexural slip is activated between them within the cover. For visualisation purposes such layers are coloured in groups of 2 in the model results.

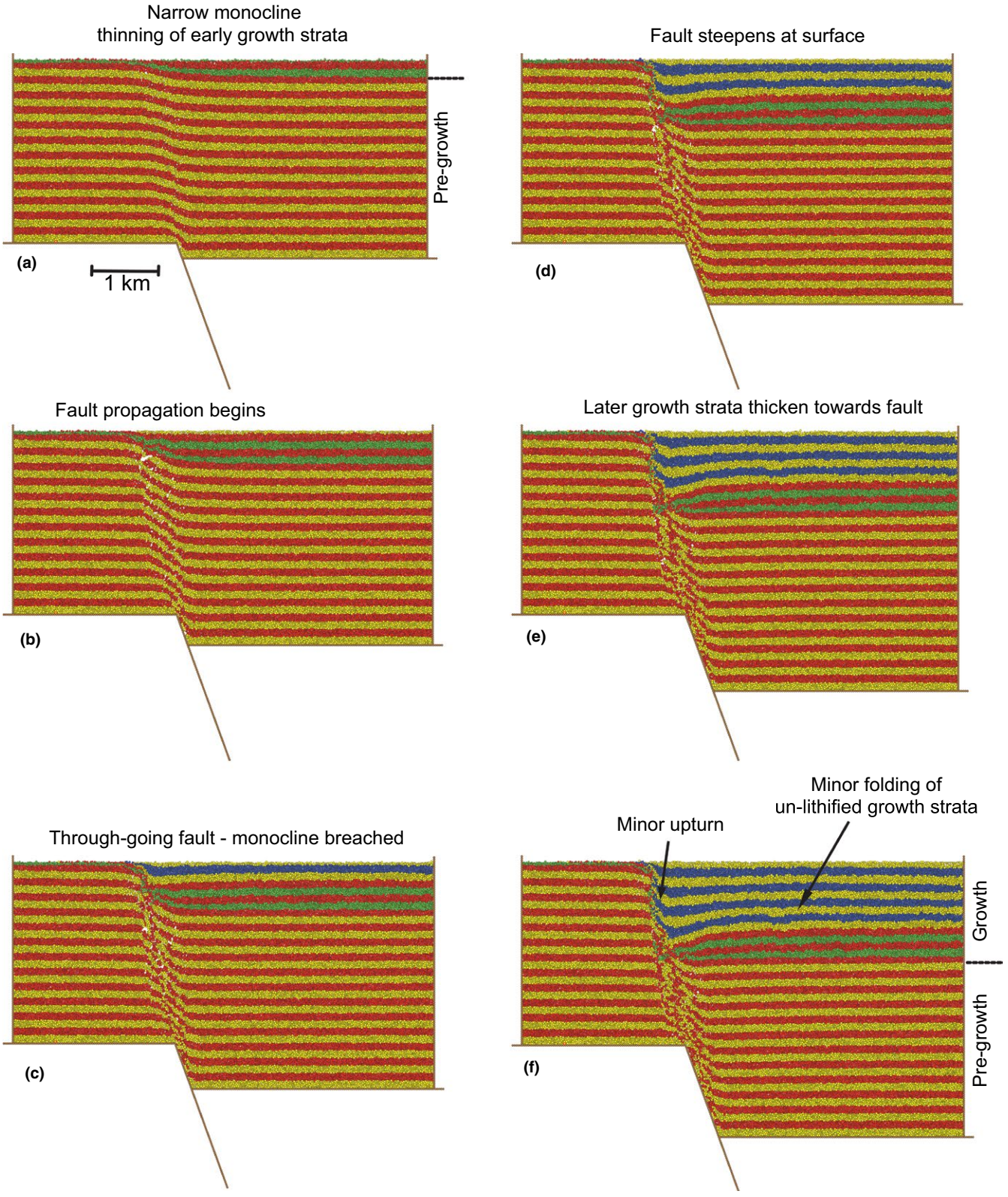

FIGURE 3 Experiment 2: a simple homogeneous elastic fault-propagation simulation. Model results shown at (a) 250, (b) 500, (c) 750, (d) 1,000, (e) 1,250 and (f) 1,500 m displacement on basement fault. Distance scale shown, no vertical exaggeration. Pregrowth strata are coloured yellow and red. Two growth strata sequences are highlighted; an early package (coloured green and red) and a later one (coloured yellow and blue)

These discrete elements obey Newton's equations of motion and interact with each other under the influence of gravity. Elements can be bonded and/or experience Mohr-Coulomb frictional contact interactions with their neighbours (see Finch et al., 2004; Hardy et al., 2009 for a full description of the modelling approach). In discrete element models such as

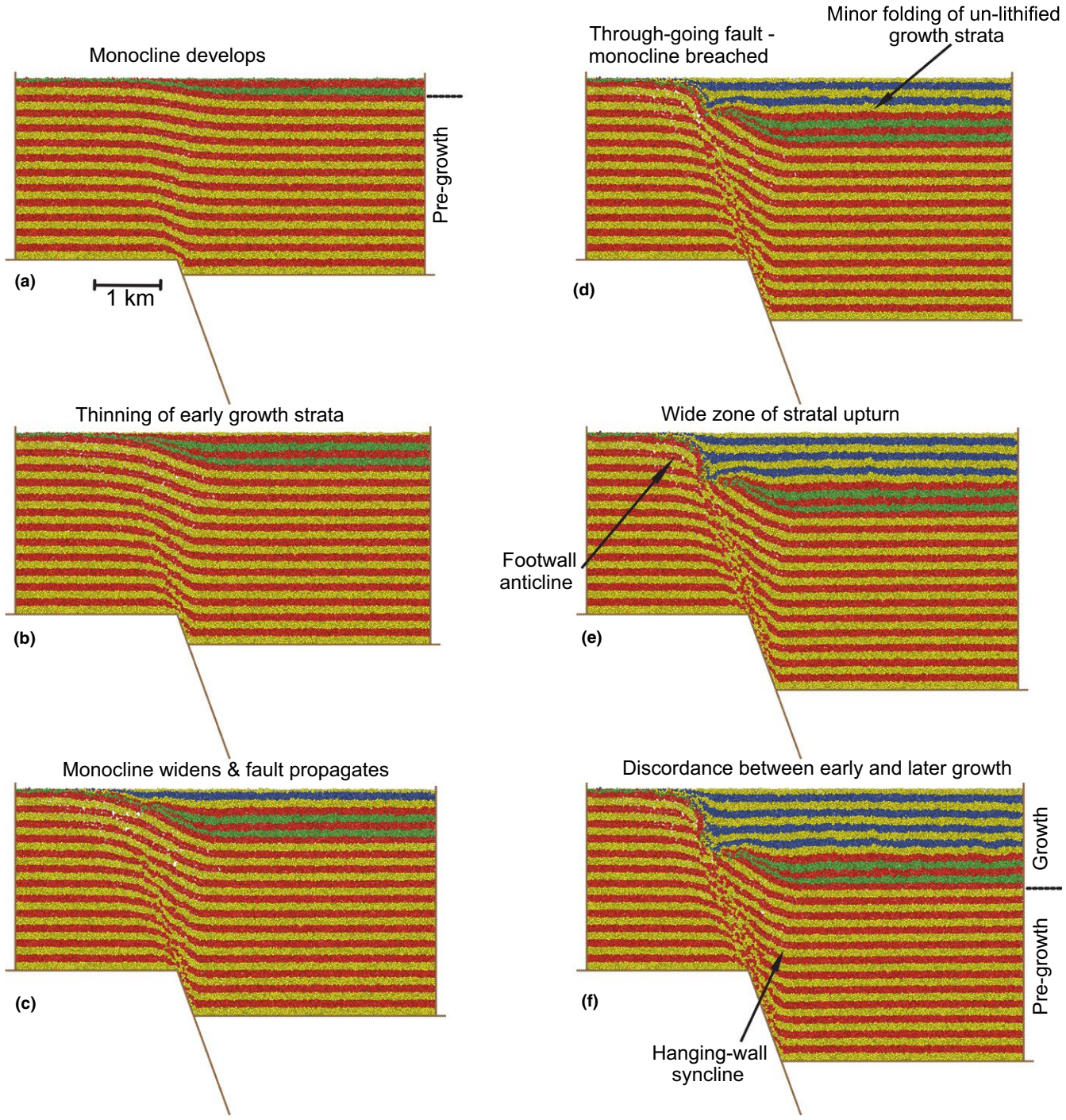

FIGURE 4 Experiment 3: A flexural-slip elastic fault-propagation simulation. Model results shown at (a) 250, (b) 500, (c) 750, (d) 1,000, (e) 1,250 and (f) 1,500 m displacement on basement fault. Distance scale shown, no vertical exaggeration. Pregrowth strata are coloured yellow and red. Two growth strata sequences are highlighted; an early package (coloured green and red) and a later one (coloured yellow and blue)

that used here the parameters such as strength, coefficient of friction etc, of an assemblage are emergent properties and do not relate directly to micro-properties. They are typically assessed through the use of angle of repose and/or unconfined/confined biaxial numerical tests (cf. Oger et al., 1998; Finch et al., 2004; Holohan et al., 2011; Botter et al., 2014). Using such tests, the frictional-cohesive discrete elements used here have been found to have a bulk coefficient of friction (μ) of c. 0.70 (internal angle of friction [ϕ] of c. 35°) and to have a cohesion of c. 2.8 MPa. The bonded elastic assemblages used here have been found to have a bulk unconfined compressive strength (UCS) of c. 23.0 MPa. The Young's modulus (E) of the bonded elastic assemblage is approximately 1.0–1.3 GPa. The un-bonded elastic assemblages have a bulk unconfined compressive strength (UCS) of c. 2.0 MPa. Unconfined compressive tests of the frictional-cohesive, elastic bonded and

weak (un-bonded) growth materials are shown in Figure 1e and are summarised in Table 1. Clearly, the strength of a heterogenous, layered material in any uniaxial or biaxial test will depend on the orientation of the layering with respect to the maximum compressive stress. However, the flexural-slip model used here has essentially a mixed rheology and thus will be weaker than the simple elastic model but stronger than the un-bonded elastic material. These strength values lie within the ranges reported for natural sedimentary rock masses at a metric scale and are much smaller than those typically derived from centimetre-scale laboratory samples (cf. Schultz, 1996; Strayer, Erickson, & Suppe, 2004; Holohan et al., 2011), but do lie within the ranges reported for natural rock masses (cf. Schultz, 1996; Strayer et al., 2004; Holohan et al., 2011) and are within the range of values used in previous discrete element studies (e.g. Holohan et al., 2011; Smart & Ferrill, 2018).

The applied (incremental) basement fault displacement in each experiment is transmitted to the cover, changing local element interactions and thus contact forces. As a result of the change in local forces, the internal elements are advanced to their new positions within the model by integrating their equations of motion using Newtonian physics and a velocity-Verlet based numerical scheme (cf. Mora & Place, 1993). Element positions are saved during experiments to allow a detailed, high-resolution analysis of geometry, displacement and strain (cf. Cardozo & Allmendinger, 2009). The numerical code used (cdem2D) has been parallelised using OpenMP and has been thoroughly tested and verified against the serial version (cf. Chapman, Jost, & Pas, 2007; Hardy, 2015). Typical experiments like those discussed here take ca. 12 hr to run on a desktop machine with two 6-core Intel Xeon (X5650—2.66 GHz) processors allowing 24 computational threads. Model results are presented at regular intervals throughout as 'time snapshots'.

TABLE 1 Experimental numerical model parameters

	Numerical model
Initial model width (km)	6.25
Initial model height (km)	2.77
Element density (kg/m^3)	2,500.0
Number of pregrowth elements	c. 46,000
Total number of pregrowth and growth elements	c. 100,000
Average element radius (m)	9.5
Frict-cohesive cover—angle of friction (deg)	35
Frict-cohesive cover—cohesion (MPa)	2.8
Bonded elastic cover—UCS (MPa)	23
Bonded elastic cover—young's modulus (GPa)	1.0–1.3

For each experiment discussed herein many different models have been run with parameters similar to those described above. However, the specific experiments discussed are representative of the stratigraphic and structural evolution typically observed under these boundary conditions in that they contain the reproducible, characteristic features seen in many models. In a manner similar to outcrop examples, seismic data or analogue models determining the 'representativeness' or generality of any geometries observed in a specific, presented model are, in a sense, subjective. The important scientific message to be taken away is not thus the precise location of an individual geometric feature or fault, but rather the distinctive, reproducible, structural behaviour and stratigraphic sequences that emerge from multiple experiments. All results are shown after 250, 500, 750, 1,000, 1,250 and 1,500 m displacement on the basement fault. Two distinct growth packages are highlighted/coloured in order to show the stratal architectures developed in early (red-green package) and mid/later (yellow-blue package) fault growth, the transition occurs at 475 m basement fault slip—chosen as it best highlights the distinct difference between fold-related growth strata and fault-related growth strata in all experiments.

3 | NUMERICAL EXPERIMENT RESULTS

3.1 | Experiment 1. Basement normal fault with a cohesive-frictional pregrowth cover sequence

The first experiment shown here is presented to illustrate the type of result obtained when the (pre-growth) cover material is simply treated as frictional-cohesive. This would be similar to many of the analogue experiments run using sand and other granular, frictional materials (e.g. Horsfield, 1977; Vendeville, 1988; McClay, 1990). The growth materials in this model are considered to be un-bonded elastic and are thus much weaker than the pregrowth materials. Overall in this experiment, one can observe that a monocline per se does not develop in the cover, but rather there is a narrow, upward-widening zone of faulting between the footwall and hanging-wall of the basement fault (Figure 2). In addition, neither a hanging-wall syncline nor a footwall anticline are produced. The temporal evolution of structural development can be summarised as follows: after 250 m displacement, the basement fault is linked to two, nearly through-going, normal faults in the cover; an earlier, steeper, fault and a later fault that dips at approximately 70 degrees (Figure 2a). At this stage there is no monocline or fold, but rather an upwards-widening zone of faulting. Faults in this frictional-cohesive cover propagate rapidly towards the free surface. This results in differential subsidence from footwall to hanging-wall and

in a thinning of the early growth strata towards the footwall (Figure 2a). This is quickly followed however (after 500 m displacement, Figure 2b) by one major through-going fault that takes up nearly all displacement in the cover. Thus, there is no longer any differential subsidence or thinning of growth strata towards the footwall (Figure 2b). Due to both the rapid propagation of the faults in the cover and the very weak nature of the growth strata there is no visible faulting in the growth strata. With 750 m displacement on the basement fault this pattern of deformation continues (Figure 2c) but we now see the development of an antithetic fault in the hanging-wall and some thickening of growth strata towards the footwall. The antithetic fault forms as a result of the upwards-steepening nature of the main cover fault. One can note that there is no major upturning of beds against the fault, but rather we see a set of almost horizontal strata separated by discrete faults. There is also no angular discordance between the early growth strata (coloured green and red) and later growth strata (coloured yellow and blue; Figure 2c). This pattern essentially continues for the rest of the model evolution (Figure 2d–f); in the youngest growth strata there is slight upturn (and thus thinning) immediately adjacent to the fault but it is not remarkable (Figure 2e,f). In addition, there is some thickening in upper growth strata as the fault steepens slightly near the free surface (Figure 2f). Note that because the growth strata are considered to be un-lithified and thus very weak, low amplitude folding is produced in the growth section.

3.2 | Experiment 2. Basement normal fault with a homogeneous, elastic pregrowth cover sequence

The second experiment shown here is given to illustrate the type of result obtained when the pregrowth cover material is simply treated as bonded elastic, strong and homogeneous. This is shown to illustrate what would happen if all pregrowth layers possessed the same strength but no flexural slip was allowed at layer interfaces (i.e. bonding is homogenous). This type of rheology might be equivalent to a strong, lithified and homogenous sandstone or limestone sequence. This model is analogous to many of the experiments run in previous numerical studies, where results were interesting but failed to produce major hanging-wall synclines and did not include growth strata (e.g. Finch et al., 2004). The growth strata are considered, as above, to be un-bonded elastic and are thus much weaker than the pregrowth. Overall in this experiment, in contrast to the frictional-cohesive case, one can observe that a narrow monocline *does* develop in the cover above the basement fault (Figure 3). The temporal evolution of structural development can be summarised as follows: a narrow monocline develops above the basement fault early in the model evolution (after 250 m displacement; Figure 3a), with noticeable thinning over it apparent in the early growth strata. However, the monocline is breached quite quickly as the basement fault propagates towards the surface linking with higher-level fractures and faults (Figure 3b,c). The monocline does not noticeably widen outward or upwards and its limb achieves a maximum dip of approximately 25–30 degrees. This early evolution is followed by a phase of localised deformation on one main fault with thickening in the later growth strata as this fault steepens near the free surface (Figure 3d–f). There is clearly a distinction between the nature of the different growth sections and some upturn against the fault but the zone of deformation is neither wide nor upwards-widening. In addition, only minor footwall syncline and hanging-wall anticlines are produced. As before, as the growth strata are considered to be un-lithified and very weak, low amplitude folding is produced in the growth section.

3.3 | Experiment 3. Basement normal fault with a layered, heterogenous elastic cover sequence

The third experiment shown here is given to illustrate the type of result obtained when the cover material is not simply treated as homogeneous elastic, but rather flexural slip is allowed to occur at the interfaces between all (defined) elastic layers. This can be considered to be the equivalent of modelling a heterogenous layered package where a series of strong sandstone or limestones units are separated by a series of very weak thin interfaces (eg., shales). As before, the growth strata are considered to be un-bonded elastic and are thus much weaker than the bonded pregrowth. Overall, one can observe that a *major* monocline develops in this experiment and is subsequently breached. The temporal evolution of structural development can be summarised as follows: a prominent monocline develops early in the model evolution (after 250 m displacement; Figure 4a). This monocline noticeably widens outwards and upwards, with pregrowth beds steepening downwards (from 10 to 35 degrees) towards the basement fault tip. In addition, there is very obvious thinning of early growth strata towards and over the monocline (Figure 4a). However, with continued basement fault displacement, the monocline steepens and the fault begins to propagate towards the surface (Figure 4b,c), although much slip is still accommodated along the layer interfaces. Pregrowth strata now steepen from 20 degrees downwards reaching 45 degrees near the fault tip (Figure 4c). The monocline is now significantly wider than before (Figure 4c) and while growth strata still thin towards it we now see that early growth strata are rotated and steeped and then overstepped by later growth strata. After 1 km displacement on the basement fault the monocline is finally breached (Figure 4d) and the early phase of folding is followed by a phase of localised displacement on one main fault (Figure 4d–f). This breaching of the monocline leaves a

wide zone of rotated/folded pregrowth strata adjacent to the fault (Figure 4d) in the form of a major hanging-wall syncline (up to 1.3 km wide) and minor footwall anticline (up to 750 m wide); both are significantly wider than the small folds seen in Expts. 1 and 2. From this stage onwards we observe that there is no major thinning or thickening of later growth strata towards the footwall. As before, the growth strata are considered to be un-lithified and very weak and thus low amplitude folding is produced in the growth section. Both pregrowth and early growth strata are also upturned and then unconformably overlapped by later growth strata (Figure 4d–f). Note the very distinctive progressive fanning of growth strata from steep but parallel to pregrowth strata to sub horizontal (Figure 4f). The final geometry produced in this model is strikingly different to the two previous experiments; in particular note the angular unconformity between the pregrowth and growth strata, the width of the folds in the pregrowth and growth sequences and the degree of secondary faulting.

4 | DISCUSSION

The three models shown above have given some insight into the effect that the rheology of cover materials can have on the geometry and evolution of extensional fault-propagation folds. They also show the manner in which growth strata 'record' the evolution of such structures. Clearly, the final geometry produced in each of these three experiments is quite different (Figures 2f, 3f, 4f) and they are all able to simulate extensional fault-propagation folds to varying degrees. A very commonly used rheology in numerical and analogue modelling studies, a frictional-cohesive cover, does not produce a characteristic *monocline* at all but rather a zone of distributed faulting over which growth strata thin. In addition, no hanging-wall syncline or footwall anticline develops and there is no major rotation/upturn of strata into the fault zone (Figure 2) as deformation is dominated by faulting. A simple, homogenous, elastic cover sequence, another commonly used cover rheology, produces a narrow monocline, thinning of early growth strata towards the fault zone but only a minor hanging-wall syncline and footwall anticline (Figure 3). However, models that incorporate mechanical stratigraphic variability (e.g. Smart & Ferrill, 2018) lead to very different results than models with a homogeneous cover. In the study presented here, the use of a cover in which flexural slip is facilitated (via un-bonded multilayer interfaces) produces both major stratal upturn towards the fault zone, a hanging-wall syncline/footwall anticline and complex thinning and truncation relationships within growth strata (Figure 4; cf. Figure 1). Thus, if we are trying to simulate and understand the evolution of extensional fault-propagation folds in nature and seismic, these results provisionally suggest that some method of including flexural slip in either numerical or analogue modelling studies is essential. This is not to suggest that some cover materials cannot be adequately simulated using either homogenous frictional-cohesive or elastic but rather that, in many examples, mechanical heterogeneity is very important (cf. Corfield & Sharp, 2000; Jackson et al., 2006; Lewis, Jackson, Gawthorpe, & Whipp, 2015; Conneally, Childs, & Nicol, 2017).

In these initial models the growth strata included have been considered to be very weak (without friction, cohesion or bonding) and thus behave quite differently to the underlying pregrowth sequence, leading to a degree of decoupling of the growth from the pregrowth sequence. I will now present three complementary, additional models (see Figure 5) where the growth strata are now assumed to have *similar* material properties to the pregrowth strata; meaning that they have the same bonding style, coefficient of friction and cohesion. However, due to their position in the cover, packing etc. they will not be statistically *identical* to the pregrowth strata but will have very similar strength and material behaviour. This can be considered to be one end-member scenario whereby early lithification takes place and the growth strata are thus much more coupled to the pregrowth strata. This is not an unreasonable scenario as in these models the final displacement on the basement fault is 1.5 km, which with reasonable, reported, slip rates may take approximately 1 Ma to accrue (see Hardy, 1994). It might be expected that during this time much of the growth sequence would become lithified, either through cementation or compaction. The final model geometries after 1.5 km of basement faulting for both the lithified and un-lithified experiments are show in Figure 5. In each of these three models one can see that the inclusion of growth strata that are as strong as the pregrowth strata has a quite significant effect upon fold growth, stratal thickening and final geometry. In each case, the inclusion of strong growth strata leads to geometries that are much more similar/consistent between growth and pregrowth. In the frictional-cohesive case (Figure 5a) this also allows some propagation of the antithetic fault into the growth section and the suppression of any low amplitude folding. In addition, in the upper growth sequence (coloured blue and yellow) the measured maximum thickness, compared to the far-field thickness (1,000 m), decreases by c. 10%. In the case of the homogeneous elastic model (Figure 5b) there is now no major expansion of the growth sequence towards the fault and early growth strata no longer turn downward towards the fault; as a result the upper growth sequence (coloured blue and yellow), compared to the far-field thickness, decreases by c. 15%. Finally, in the case of flexural slip (Figure 5c), the overall effect is one of a slight decrease in the dip of the upturned hanging-wall strata; the upper growth sequence do not change maximum thickness to any significant extent. However, many of the basic relationships remain the same, although folding within the growth strata is suppressed and strata are much more parallel. In

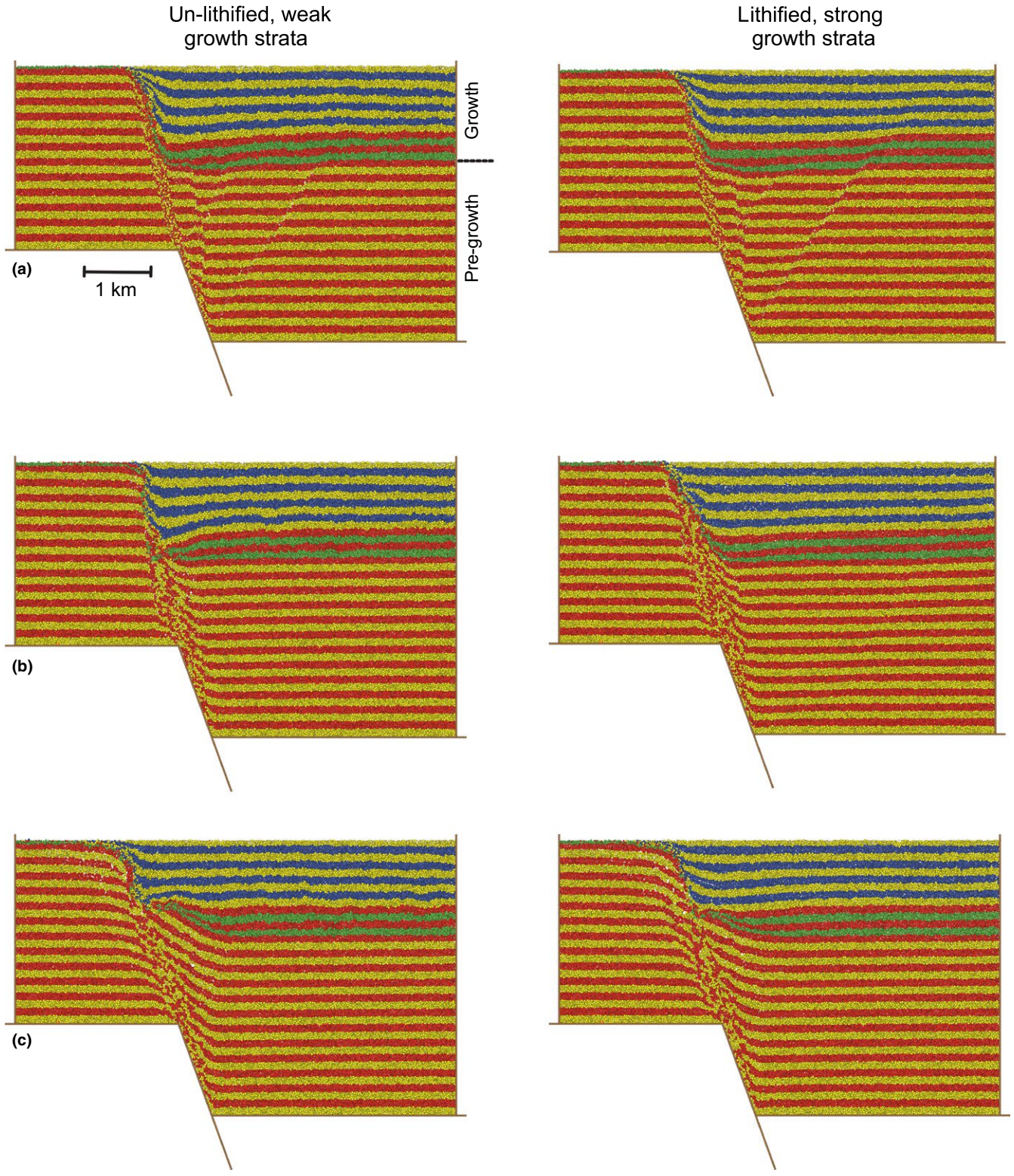

FIGURE 5 Experiments 1 (a), 2 (b) and 3 (c) with weak growth strata (left column) compared with identical models where the growth strata are as strong as the pregrowth (right column). Model results shown at 1,500 m displacement on basement fault. Distance scale shown, no vertical exaggeration. Pregrowth strata are coloured yellow and red. Two growth strata sequences are highlighted; an early package (coloured green and red) and a later one (coloured yellow and blue)

many ways these effects are logical, in that including a strong, lithified growth sequence above a growing fault/fold imposes a very different boundary/loading condition, increases stress at depth and thus partly conditions the path of deformation. A weak growth sequence is much easier to deform and thus in many ways, the fold is more free to develop, less constrained

and the growth sequence is to an extent decoupled. The sequential addition of strong growth strata is conceptually similar to imposing a horizontal upper surface to the model repeatedly. In this case the growth sequence is much more coupled to the pregrowth sequence. Regardless of the particular rheology used for growth strata, it is clear that growth strata do not only 'record' fold and fault growth but can also *influence* it as well. Thus, they are not just 'passive' recorders of fold and fault growth. Also, whilst the differences between geometries may not be dramatic, as always the 'Devil is in the detail' and one may look for the subtle difference in possible stratigraphic and structural traps between both end-members. This is particularly important in many subsurface examples of extensional fault-propagation folds where there is often limited seismic resolution and limited well data. As a result, predicting the geometry/architecture, thickness and location of both pregrowth and growth reservoirs can prove difficult (e.g. Corfield & Sharp, 2000; Jackson et al., 2006; Lewis et al., 2015).

The approach used here to simulate or 'promote' flexural slip between defined layers in the cover materials is probably one of the simplest possible. However, it does illustrate well the characteristics of such a deformation mechanism and its influence upon fault-related fold growth and final structural and stratigraphic geometries. Clearly, with higher numerical resolution and many more layers than the 48 used here (in the pregrowth), finer-scale structures and features would form but the basic geometries produced would not be altered radically. Such very-high resolution models are now becoming tractable with today's computing power and parallelisation; as long as numerical stability is ensured, such large numbers of elements do not present any real computational problem. In addition, this approach is not the first or only manner to introduce mechanical heterogeneity into a cover sequence, another option would be, e.g., to introduce multiple weak and strong *layers* rather than just weak interfaces between many strong layers (e.g. Finch et al., 2004; Smart & Ferrill, 2018), in many ways the field data may condition the approach used (cf. Smart & Ferrill, 2018). Regardless of the specific approach used, the inclusion of flexural slip into the modelling scheme produces results which appear to be strikingly similar to many seen in nature and in seismic (Figure 1a–c; Figure 4, Figure 5c). This is not to say that *all* cover sequences deform like this, some may well behave in a manner which is closer to the frictional-cohesive or elastic models.

This brings us to the application of kinematic models to extensional fault-propagation folds. Models based on kink-band modelling are not particularly appropriate to such structures with their curved limbs and downward steepening strata. Thus, over the past 20 years the trishear model has been widely adopted to explain many aspects of the geometry and kinematics of such fault propagation-folds (Allmendinger, 1998; Erslev, 1991; Hardy & McClay, 1999; Jin & Groshong, 2006; Khalil & McClay, 2002; Zhao et al., 2017). Clearly, trishear can reproduce, with some *geometric* accuracy, many of the key features seen in such folds (Allmendinger, 1998; Hardy & McClay, 1999; Jin & Groshong, 2006; Khalil & McClay, 2002; Zhao et al., 2017). Also strain prediction based on the trishear velocity field can provide an estimation of the magnitude and orientation of the strain ellipses in the cover. In particular, lines of no finite elongation (LNFE) appear to be good predictors of the orientations of second-order faults as proposed by Allmendinger (1998). However, the parameters that constrain/define trishear: P/S, apical angle, the concentration factor etc., are poorly constrained and we, to date, have no idea what these parameters relate to in nature. Thus, a question still remains as to what exactly trishear is modelling. This is perhaps partly due to the fact that any kinematic model only produces continuous deformation and relating this to the discontinuous (metric scale) deformation seen in the field can prove difficult. The results presented here perhaps also suggest, where we have a well-layered, mechanically heterogeneous cover with many potential slip planes, trishear in this setting perhaps reproduces the manner in which flexural slip is progressively activated upwards and outwards from a fault-tip singularity. This interpretation was alluded to previously by Conneally et al. (2017; their Figure 1a). Khalil and McClay (2002) also noted that wide trishear angles, where one of the boundaries of the trishear zone is sub-parallel to bedding, simulate the development of layer-parallel flexural-slip deformation. In addition, this study has illustrated that materials used in laboratories and numerical models much be chosen extremely carefully. In many situations a frictional-cohesive material may produce very appropriate/pleasing results when simulating faulting rather than folding; however, when comparing to natural examples, field data need to drive the choice of rheology.

Finally, the approach to modelling extensional fault-propagation folds presented here is neither unique nor complete but it does show the power of the discrete element technique in tackling geological problems with abrupt or changing boundary conditions and where both folding and faulting are key features. In this initial study, I have also not included much more complicated mechanical stratigraphies (both vertically and laterally), but in principle this is not an issue. The model of growth sedimentation used here is also extremely simple and does not include base level change and/or erosion, however recent advances mean that much more complete models of sedimentation per se can now be incorporated into the model (cf. Hardy, 2018b). The model presented here is also 2D and obviously natural faults and folds grow in 3D. Finally, the influence of progressively lithifying growth strata with depth through time may well have a significant influence of fold growth and geometry. These and other topics are subjects of ongoing research.

5 | CONCLUSIONS

While simple, homogenous, frictional-cohesive or elastic rheological models can be used to simulate many features of the upper crust, they fail to appropriately reproduce some of the key features/deformation mechanisms seen in natural examples of extensional fault-propagation folds. This is particularly so when the cover stratigraphy is mechanically heterogeneous and where footwall anticlines, hanging-wall synclines and complex growth stratal records of fold growth are typically all present. Thus, variable layer properties and/or interlayer slip may well be the most geologically realistic approach to incorporating mechanical stratigraphy into such simulations. These features are much better simulated when mechanical heterogeneity and/or flexural slip is included in a modelling scheme such as in the discrete element model presented here. The use of a cover in which flexural slip is facilitated (via un-bonded multilayer interfaces) produces both major stratal upturn towards the fault zone, a hanging-wall syncline/footwall anticline and complex thinning and truncation relationships within growth strata (Figure 4; cf. Figure 1). The resultant breached monoclines and their growth strata are strikingly similar to those seen in nature. If we are trying to simulate and understand the evolution of extensional fault-propagation folds in nature and seismic, these results suggest that some method of including mechanical stratigraphy and/or flexural slip in either numerical or analogue modelling is essential. Both un-lithified and lithified growth strata have been considered and clearly show the effect that growth strata *themselves* can have on fault-related fold growth. Thus, they are not just 'passive' recorders of fold and fault growth. A final suggestion of this study is that, in this setting, trishear perhaps encapsulates the geometric expression of a widening zone of flexural slip activation away from a fault tip singularity.

ACKNOWLEDGMENTS

Discussions with, and the patience of, many colleagues over many years is appreciated; I particularly thank Dave Waltham for stimulating my interest in numerical modelling many years ago. Comments by the Editor Atle Rotevatn and the three reviewers have greatly helped to improve the manuscript. Discrete element modelling was carried out using cdem2D by the author.

REFERENCES

Allen, M. P., & Tildesley, D. J. (1987). *Computer simulation of liquids*. Oxford, UK: Oxford Science Publications.

Allmendinger, R. W. (1998). Inverse and forward numerical modelling of trishear fault-propagation folds. *Tectonics*, *17*, 62–81.

Botter, C., Cardozo, N., Hardy, S., Lecomte, I., & Escalona, A. (2014). From mechanical modeling to seismic imaging of faults: A synthetic workflow to study the impact of faults on seismic. *Marine and Petroleum Geology*, *57*, 187–207. https://doi.org/10.1016/j.marpetgeo.2014.05.013

Botter, C., Cardozo, N., Hardy, S., Lecomte, I., Paton, G., & Escalona, A. (2016). Seismic characterisation of fault damage in 3D using mechanical and seismic modelling. *Marine and Petroleum Geology*, *77*, 973–990. https://doi.org/10.1016/j.marpetgeo.2016.08.002

Cardozo, N., & Allmendinger, R. W. (2009). SSPX: A program to compute strain from displacement/velocity data. *Computers & Geosciences*, *35*, 1343–1357. https://doi.org/10.1016/j.cageo.2008.05.008

Cardozo, N., Jackson, C., & Whipp, P. (2011). Determining the uniqueness of best-fit trishear models. *Journal of Structural Geology*, *33*, 1063–1078. https://doi.org/10.1016/j.jsg.2011.04.001

Chapman, B., Jost, G., & van der Pas, R. (2007). *Using OpenMP: Portable shared memory parallel programming*. Cambridge, MA: The MIT Press.

Conneally, J., Childs, C., & Nicol, A. (2017). Monocline formation during growth of segmented faults in the Taranaki Basin, offshore New Zealand. *Tectonophysics*, *721*, 310–321. https://doi.org/10.1016/j.tecto.2017.06.036

Corfield, S., & Sharp, I. R. (2000). Structural style and stratigraphic architecture of fault propagation folding in extensional settings: A seismic example from the Smørbukk area, Halten Terrace, Mid-Norway. *Basin Research*, *12*, 329–341.

Cundall, P. A., & Strack, O. D. L. (1979). A discrete numerical model for granular assemblies. *Geotechnique*, *29*, 47–65. https://doi.org/10.1680/geot.1979.29.1.47

Egholm, D. L., Sandiford, M., Clausen, O. R., & Nielsen, S. B. (2007). A new strategy for discrete element numerical models: 2. Sandbox applications. *Journal of Geophysical Research*, *112*, B05204. https://doi.org/10.1029/2006JB004558

Erslev, E. A. (1991). Trishear fault-propagation folding. *Geology*, *19*, 617–620.

Ferrill, D. A., & Morris, A. P. (2008). Fault zone deformation controlled by carbonate mechanical stratigraphy, Balcones fault system. *Texas. AAPG Bulletin*, *92*, 359–380. https://doi.org/10.1306/10290707066

Ferrill, D. A., Morris, A. P., & McGinnis, R. N. (2012). Extensional fault propagation folding in mechanically layered rocks: The case against a frictional drag mechanism. *Tectonophysics*, *576–577*, 78–85.

Ferrill, D. A., Morris, A. P., & Smart, K. J. (2007). Stratigraphic control on extensional fault propagation folding: Big Brushy Canyon monocline, Sierra Del Carmen, Texas. *Geological Society, London, Special Publications*, *292*, 203–217. https://doi.org/10.1144/SP292.12

Finch, E., Hardy, S., & Gawthorpe, R. L. (2004). Discrete-element modelling of extensional fault-propagation folding above rigid basement fault blocks. *Basin Research*, *16*, 467–488. https://doi.org/10.1111/j.1365-2117.2004.00241.x

Ford, M., Carlier, L. e., de Veslud, C., & Bourgeois, O. (2007). Kinematic and geometric analysis of fault-related folds in a rift setting: The Dannemarie basin, Upper Rhine Graben, France. *Journal of Structural Geology*, *29*, 1811–1830. https://doi.org/10.1016/j.jsg.2007.08.001

Grant, J. V., & Kattenhorn, S. A. (2004). Evolution of vertical faults at an extensional plate boundary, southwest Iceland. *Journal of Structural Geology*, *26*, 537–557. https://doi.org/10.1016/j.jsg.2003.07.003

Hardy, S. (1994). *Mathematical modelling of sedimentation in active tectonic settings*. PhD thesis, Royal Holloway University of London.

Hardy, S. (2008). Structural evolution of calderas: Insights from two-dimensional discrete element simulations. *Geology*, *36*, 927–930. https://doi.org/10.1130/G25133A.1

Hardy, S. (2011). Cover deformation above steep, basement normal faults: Insights from 2D discrete element modeling. *Marine and Petroleum Geology*, *28*, 966–972. https://doi.org/10.1016/j.marpetgeo.2010.11.005

Hardy, S. (2015). The Devil truly is in the detail. A cautionary note on computational determinism: Implications for structural geology numerical codes and interpretation of their results. *Interpretation*, *3*(4), SAA29–SAA35. https://doi.org/10.1190/INT-2015-0052.1

Hardy, S. (2016). Does shallow dike intrusion and widening remain a possible mechanism for graben formation on Mars? *Geology*, *44*, 107–110. https://doi.org/10.1130/G37285.1

Hardy, S. (2018a). Coupling a frictional-cohesive cover and a viscous substrate in a discrete element model: First results of application to thick- and thin-skinned extensional tectonics. *Marine and Petroleum Geology*, *97*, 32–44. https://doi.org/10.1016/j.marpetgeo.2018.06.026

Hardy, S. (2018b). Novel discrete element modelling of Gilbert-type delta formation in an active tectonic setting—First results. *Basin Research*, 1–15. https://doi.org/10.1111/bre.12309

Hardy, S., & McClay, K. (1999). Kinematic modelling of extensional fault-propagation folding. *Journal of Structural Geology*, *21*, 695–702. https://doi.org/10.1016/S0191-8141(99)00072-3

Hardy, S., McClay, K., & Muñoz, J. A. (2009). Deformation and fault activity in space and time in high-resolution numerical models of doubly vergent thrust wedges. *Marine and Petroleum Geology*, *26*(2), 232–248.

Holohan, E. P., Schopfer, M. P. J., & Walsh, J. J. (2011). Mechanical and geometric controls on the structural evolution of pit crater and caldera subsidence. *Journal of Geophysical Research*, *116*, B07202. 1029/2010JB008032

Horsfield, W. T. (1977). An experimental approach to basement-controlled faulting. *Geologie En Mijnbouw*, *56*, 363–370.

Jackson, C. A. L., Gawthorpe, R. L., & Sharp, I. R. (2006). Style and sequence of deformation during extensional fault-propagation folding: Examples from the Hammam Faraun and El-Qaa fault blocks, Suez Rift, Egypt. *Journal of Structural Geology*, *28*, 519–535. https://doi.org/10.1016/j.jsg.2005.11.009

Jin, G., & Groshong, R. H. (2006). Trishear kinematic modelling of extensional fault-propagation folding. *Journal of Structural Geology*, *28*, 170–183.

Johnson, K. M., & Johnson, A. M. (2002a). Mechanical models of trishear-like folds. *Journal of Structural Geology*, *24*, 277–287.

Johnson, K. M., & Johnson, A. M. (2002b). Mechanical analysis of the geometry of forced-folds. *Journal of Structural Geology*, *24*, 401–410.

Kane, K. E., Jackson, C.-A.-L., & Larsen, E. (2010). Normal fault growth and fault-related folding in a salt-influenced rift basin: South Viking Graben, offshore Norway. *Journal of Structural Geology*, *32*, 490–506. https://doi.org/10.1016/j.jsg.2010.02.005

Keller, J. V. A., & Lynch, G. (2000). Displacement transfer and forced folding in the Maritimes basin of Nova Scotia, eastern Canada. In J. W. Cosgrove, & M. S. Ameen (Eds.), *Forced folds and fractures* (pp. 87–101). Geological Society London Special Publication, 169.

Khalil, S. M., & McClay, K. R. (2002). Extensional fault-related folding, northwestern, Red Sea, Egypt. *Journal of Structural Geology*, *24*, 743–762. https://doi.org/10.1016/S0191-8141(01)00118-3

Lăpădat, A., Imber, J., Yeilding, G., Iacopini, D., McCaffrey, K., Long, J. J., & Jones, R. R. (2016). *Occurrence and development of folding related to normal faulting within a mechanically heterogeneous sedimentary sequence: A case study from Inner Moray Firth UK*. Geological Society, London, Special Publication 439.

Lewis, M. M., Jackson, C.-A.-L., & Gawthorpe, R. L. (2013). Salt-influenced normal fault growth and forced folding: The Stavanger Fault System, North Sea. *Journal of Structural Geology*, *54*, 156–173. https://doi.org/10.1016/j.jsg.2013.07.015

Lewis, M. M., Jackson, C.-A.-L., Gawthorpe, R. L., & Whipp, P. S. (2015). Early synrift reservoir development on the flanks of extensional forced folds: A seismic-scale outcrop analog from the Hadahid fault system, Suez rift, Egypt. *AAPG Bulletin*, *99*(06), 985–1012. https://doi.org/10.1306/12011414036

Maurin, J. C., & Niviere, B. (2000). Extensional forced folding and dècollement of the pre-rift series along the Rhine graben and their influence on the syn-rift sequences. In J. W. Cosgrove, & M. S. Ameen (Eds.), *Forced folds and fractures* (pp. 87–101). Geological Society London Special Publication, 169.

McClay, K. R. (1990). Extensional fault systems in sedimentary basins: A review of analogue model studies. *Marine and Petroleum Geology*, *7*, 206–233. https://doi.org/10.1016/0264-8172(90)90001-W

Mora, P., & Place, D. (1993). A lattice solid model for the non-linear dynamics of earthquakes. *International Journal of Modern Physics C*, *4*, 1059–1074. https://doi.org/10.1142/S0129183193000823

Mora, P., & Place, D. (1994). Simulation of the frictional stick-slip instability. *Pure and Applied Geophysics*, *143*, 61–87. https://doi.org/10.1007/BF00874324

Oger, L., Savage, S. B., Corriveau, D., & Sayed, M. (1998). Yield and deformation of an assembly of disks subject to a deviatoric stress loading. *Mechanics of Materials*, *27*, 189–210.

Pascoe, R., Hooper, R., Storhaug, K., & Harper, H. (1999). In A. J. Fleet, & S. A. R. Boldly (Eds.), *Petroleum geology of northwest Europe: Proceedings of the 5th conference* (pp. 83–90).

Patton, T. L. (2004). Numerical models of growth-sediment development above an active monocline. *Basin Research*, *16*, 25–39. https://doi.org/10.1111/j.1365-2117.2003.00220.x

Place, D., Lombard, F., Mora, P., & Abe, S. (2002). Simulation of the micro- physics of rocks using LSMEarth. *Pure and Applied Geophysics*, *159*, 1911–1932. https://doi.org/10.1007/s00024-002-8715-x

Schopfer, M. P. J., Childs, C., & Walsh, J. J. (2007). Two-dimensional distinct element modeling of the structure and growth of normal faults in multilayer sequences: 1. Model calibration, boundary conditions, and selected results. *Journal of Geophysical Research*, *112*(10), B10401.

Schultz, R. A. (1996). Relative scale and the strength and deformability of rock masses. *Journal of Structural Geology*, *18*, 1139–1149. https://doi.org/10.1016/0191-8141(96)00045-4

Sharp, I. R., Gawthorpe, R. L., Underhill, J. R., & Gupta, S. (2000). Fault-propagation folding in extensional settings: Examples of structural style and synrift sedimentary response from the Suez rift, Sinai, Egypt. *Geological Society of America Bulletin*, *112*, 1877–1899.

Smart, K. J., & Ferrill, D. A. (2018). Discrete element modeling of extensional fault-related monocline formation. *Journal of Structural Geology*, *115*, 82–90. https://doi.org/10.1016/j.jsg.2018.07.009

Smart, K. J., Ferrill, D. A., & Morris, A. P. (2009). Impact of interlayer-slip on fracture prediction from geomechanical models of fault-related folds. *American Association of Petroleum Geologists Bulletin*, *93*(11), 1447–1458. https://doi.org/10.1306/05110909034

Smart, K. J., Ferrill, D. A., Morris, A. P., Bichon, B. J., Riha, D. S., & Huyse, L. (2010). Geomechanical modeling of an extensional fault-propagation fold: Big Brushy Canyon monocline, Sierra Del Carmen, Texas. *AAPG Bulletin*, *94*(2), 221–240. https://doi.org/10.1306/08050908169

Strayer, L. M., Erickson, S. G., & Suppe, J. (2004). Influence of growth strata on the evolution of fault-related folds: Distinct-element models. In McClay, K. ed., "Thrust Tectonics and Hydrocarbon Systems". *American Association of Petroleum Geologists Memoir*, *82*, 413–437.

Thompson, N., Bennett, M. R., & Petford, N. (2010). Development of characteristic volcanic debris avalanche deposit structures: New insights from distinct element simulations. *Journal of Volcanology and Geothermal Research*, *192*, 191–200.

Tvedt, A. B. M., Rotevatn, A., Jackson, C.-A.-L., Fossen, H., & Gawthorpe, R. L. (2013). Growth of normal faults in multilayer sequences: A 3D seismic case study from the Egersund Basin, Norwegian North Sea. *Journal of Structural Geology*, *55*, 1–20. https://doi.org/10.1016/j.jsg.2013.08.002

van Gent, H. W., Holland, M., Urai, J. L., & Loosveld, R. (2010). Evolution of fault zones in carbonates with mechanical stratigraphy - Insights from scale models using layered cohesive powder. *Journal of Structural Geology*, *32*, 1375–1391. https://doi.org/10.1016/j.jsg.2009.05.006

Vendeville, B. C. (1988). Scale-models of basement induced-extension. *Comptes Rendus De L'académie Des Sciences*, *307*, 1013–1019.

White, I. R., & Crider, J. G. (2006). Extensional fault-propagation folds: Mechanical models and observations from the Modoc Plateau, northeastern California. *Journal of Structural Geology*, *28*, 1352–1370. https://doi.org/10.1016/j.jsg.2006.03.028

Willsey, S. P., Umhoefer, P. J., & Hilley, G. E. (2002). Early evolution of an extensional monocline by a propagating normal fault: 3D analysis from combined field study and numerical modeling. *Journal of Structural Geology*, *24*, 651–669. https://doi.org/10.1016/S0191-8141(01)00120-1

Withjack, M. O., & Calloway, J. S. (2000). Active faulting beneath a salt layer: An experimental study of the deformation in the cover sequence. *AAPG Bulletin*, *84*, 627–651.

Withjack, M. O., Olson, J., & Peterson, E. (1990). Experimental models of extensional forced folds. *AAPG Bulletin*, *74*, 1038–1054.

Zhao, H., Guo, Z., & Yu, X. (2017). Strain modelling of extensional fault-propagation folds based on an improved non-linear trishear model: A numerical simulation analysis. *Journal of Structural Geology*, *95*, 60–76. https://doi.org/10.1016/j.jsg.2016.12.009

How to cite this article: Hardy S. Discrete element modelling of extensional, growth, fault-propagation folds. *Basin Res*. 2019;31:584–599. https://doi.org/10.1111/bre.12335